Polymer Chemistry

Accepted Manuscript

ROYAL SOCIETY OF CHEMISTRY

www.rsc.org/polymers

Cite this: DOI: 10.1039/c0xx00000x

www.rsc.org/xxxxxx

ARTICLE TYPE

Synthesis and Morphological Studies of a Poly(5,6-difluorobenzo-2,1,3-thiadiazole-4,7-diyl-alt-quaterchalcogenophene) Copolymer with 7.3% Polymer Solar Cells Efficiency

Jhong-Sian Wu, Jyun-Fong Jheng, Jen-Yun Chang, Yu-Ying Lai, Kuan-Yi Wu, Chien-Lung Wang* and Chain-Shu Hsu*

Received (in XXX, XXX) Xth XXXXXXXXX 20XX, Accepted Xth XXXXXXXXX 20XX
DOI: 10.1039/b000000x

To obtain a poly(5,6-difluorobenzo-2,1,3-thiadiazole-4,7-diyl-*alt*-quaterchalcogenophene) (**P(FBT-*alt*-CP$_4$)**) copolymer with a small optical band gap (E_g), and to reach high short-circuit current (J_{sc}) in the **P(FBT-*alt*-CP$_4$)**:$PC_{71}BM$ polymer solar cells (PSCs), **P(FBT-*alt*-Se$_2$Th$_2$)**, which contains selenophene-2,5-diyl (-Se-) π-bridges, was synthesized. **P(FBT-*alt*-Se$_2$Th$_2$)** possesses a E_g of 1.56 eV and is strongly aggregated in solution. Wide angle X-ray diffraction (WAXD) and grazing incidence X-ray diffraction (GI-XRD) results revealed the high solid-state order of **P(FBT-*alt*-Se$_2$Th$_2$)** and its edge-on orientation on the substrate. It delivered a high hole mobility (μ_h) of 0.36 $cm^2V^{-1}s^{-1}$ in (organic field-effect transistors) OFETs. The strong aggregation tendency of **P(FBT-*alt*-Se$_2$Th$_2$)** caused large segregation domains in the **P(FBT-*alt*-Se$_2$Th$_2$)**:$PC_{71}BM$ thin film, as shown in the high-resolution transmission electron microscopy (HR-TEM) images. The addition of 8 v% of 1-chloronaphthalene (1-CN) effectively suppressed the aggregation and led to more homogeneous active layer morphology. The improved morphology enhanced the J_{sc} of the PSCs. A superior PCE of 7.34% with a V_{oc} of 0.70 V, a J_{sc} of 15.8 mA/cm^2, and a FF of 66.4% was delivered in the inverted **P(FBT-*alt*-Se$_2$Th$_2$)**:$PC_{71}BM$ PSCs. The strong aggregation of **P(FBT-*alt*-Se$_2$Th$_2$)** is likely related to its more straight conjugated backbone according to the theoretical calculation results of the **FBT-*alt*-Se$_2$Th$_2$** repeat unit.

Introduction

Conjugated donor-acceptor (D-A) copolymers have been recognized as high-performance materials used in bulk heterojunction (BHJ) polymer solar cells (PSCs).[1] The rapid developments in the molecular design enabled fine tuning of the molecular properties of the D-A copolymers. Along with the morphological optimization of the active layer made of blends of p-type polymers: n-type fullerenes, over 7-8 % of power conversion efficiencies (PCEs) in single-junction BHJ PSCs have been realized.[2,3] Moreover, interfacial layer modifications[4] and novel device architectures promoted the PCEs of multiple-junction BHJ PSCs to over the 9-10%.[5]

Modulation of the molecular energy levels of the D-A copolymers via replacing the chalcogenophene (CP) π-bridges, (i.e., furan-2,5-diyl (-Fu-), thiophene-2,5-diyl (-Th-) and selenophene-2,5-diyl (-Se-) groups) have been widely adopted because of the ready availability of the CP units and their significant influences on the molecular properties. In general, copolymers using -Fu- π-bridges have better solubility,[6] lower-lying highest occupied molecular orbital level (E_{HOMO}), and delivers higher open circuit voltage (V_{oc}) than their counterparts.[7] Those employing -Se- π-bridges generally possess more quinoidal character, stabilized E_{LUMO} and narrower E_g.[8, 9] Consequently, higher charge mobility (μ) in organic field-effect transistors (OFETs) and short-circuit current (J_{sc}) in BHJ PSCs were delivered by the devices utilizing the -Se- copolymers.[10]

P(FBT-*alt*-Th$_4$) in Scheme 1a is one of the poly(5,6-difluorobenzo-2,1,3-thiadiazole-4,7-diyl-*alt*-quaterchalcogenophene) (**P(FBT-*alt*-CP$_4$)**) copolymers. It has high crystallinity in the solid-state, delivered high hole mobility (μ_h) in organic field-effect transistors (OFETs) and 6.8 % power conversion efficiency (PCE) in BHJ PSCs.[11] However, due to the relatively large E_g of **P(FBT-*alt*-Th$_4$)**, the PCE of the **P(FBT-*alt*-Th$_4$)**:$PC_{71}BM$ PSCs was limited by the low J_{sc}. In the attempts to improve the performances of the **P(FBT-*alt*-CP$_4$)**, and to investigate the influences of the -Se- π-bridges to the **P(FBT-*alt*-CP$_4$)** copolymer, in this study, a novel **P(FBT-*alt*-CP$_4$)** copolymer, **P(FBT-*alt*-Se$_2$Th$_2$)**, was synthesized. Replacing the -Th- with the -Se- π-bridges effectively narrows the E_g to 1.56 eV, and resulted in high J_{sc} of the **P(FBT-*alt*-Se$_2$Th$_2$)**:$PC_{71}BM$ PSCs. The **P(FBT-*alt*-Se$_2$Th$_2$)**:$PC_{71}BM$ PSCs delivered a J_{sc} of 15.8 mA/cm^2, and a best PCE of 7.34%. However, the stronger aggregation tendency of **P(FBT-*alt*-Se$_2$Th$_2$)** resulted in large **P(FBT-*alt*-Se$_2$Th$_2$)** segregation domains in the **P(FBT-*alt*-Se$_2$Th$_2$)**:$PC_{71}BM$ active layer, as observed under high-resolution transmission electron microscopy. The process additive, 1-chloronaphthalene, was used to optimize the active layer

morphology. The significant changes in the molecular and morphological behaviors caused by the -Se- π-bridges were further scrutinized by morphological analyses and theoretical calculations. It was found that the larger atomic size of selenium improves the backbone linearity, which enhances aggregation strength and solid-state order of **P(FBT-*alt*-Se$_2$Th$_2$)**.

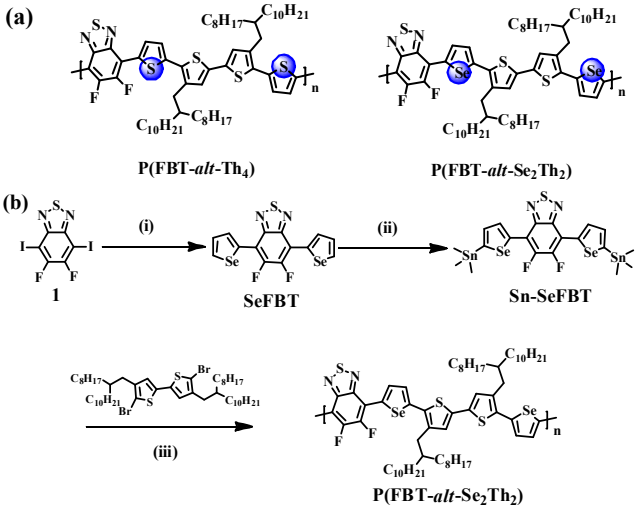

Scheme 1. (a) Chemical structures of **P(FBT-*alt*-Th$_4$)** and **P(FBT-*alt*-Se$_2$Th$_2$)**. (b) Synthetic procedures of **P(FBT-*alt*-Se$_2$Th$_2$)**. Reagents and conditions: (i) 2-(tributylstannyl)selenophene, bis(triphenylphosphine)palladium(II) dichloride, THF, 70 °C, 12 hr; (ii) LDA, dry THF, −78 °C, 1 hr; 1 M trimethyltin chloride; (iii) tris(dibenzylideneacetone)dipalladium(0), tri(o-tolyl)phosphine, chlorobenzene, 180 °C, microwave 270 W, 50 mins.

Experimental Section

General Measurement and Characterization: All chemicals are purchased from Aldrich, Lancaster, TCI or Acros used as received unless otherwise specified. ^{1}H and ^{13}C NMR spectra were measured using a 400 MHz instrument spectrometer. Differential scanning calorimeter (DSC) was measured on a TA Q200 Instrument and thermogravimetric analysis (TGA) was recorded on a Perkin Elmer Pyris under nitrogen atmosphere at a heating rate of 10 °C/min. Absorption spectra were collected on a HP8453 UV-vis spectrophotometer. The molecular weight of **P(FBT-*alt*-Se$_2$Th$_2$)** was determined with a Viscoteck HTGPC module 350, using trichlorobenzene as the eluent at 140 °C. The electrochemical cyclic voltammetry (CV) was conducted on a CH Instruments Model 611D. A Carbon glass coated with a thin polymer film was used as the working electrode and Ag/Ag$^+$ electrode as the reference electrode, while 0.1 M tetrabutylammonium hexafluorophosphate (Bu_4NPF_6) in acetonitrile was the electrolyte. CV curves were calibrated using ferrocence as the standard, whose oxidation potential is set at −4.8 eV with respect to zero vacuum level. The E_{HOMO} were deduced from the equation $E_{HOMO} = -e(E_{ox}^{onset} - E_{(ferrocene)}^{onset} + 4.8)$ eV. The E_{LUMO} levels of polymer were deduced from the equation $E_{LUMO} = -e(E_{red}^{onset} - E_{(ferrocene)}^{onset} + 4.8)$ eV.

X-ray Diffractions: The powder X-ray diffraction patterns were recorded at the BL01C2 beamline of the National Synchrotron Radiation Research Center (NSRRC) in Taiwan. The ring energy of NSRRC was operated at 1.5 GeV with a typical current of 300 mA. The wavelength of the incident X-rays was 1.033 Å (12.0 keV), delivered from the superconducting wavelength-shifting magnet, and a Si(111) double-crystal monochromator. The diffraction patterns were recorded at room temperature with a Mar345 imaging plate detector approximately 300 mm from sample positions and typical exposure duration 5 minutes. The pixel size of Mar345 was 100 μm. The one-dimensional powder diffraction profile was converted with program FIT2D and cake-type integration. The diffraction angles were calibrated according to Bragg positions of Ag-benhenate and Si powder (NBS640b) standards. The powder sample was sealed in a capillary (1.0 mm diameter); each powder XRD pattern was exposed for about 1.2 minutes. GI XRD measurements were performed at the BL23A end station of the NSRRC, Taiwan. Sample thin films were prepared by spin-casting the copolymer solutions (2.7mg dissolved in 0.5mL of ODCB) on Si wafers at 500 rpm. The thin films were then annealed at 200 °C for 1 hr. The samples were then placed horizontally on a stage enclosed in an airtight chamber with thin (8 μm) Kapton windows for X-rays. With a 8.0 keV (wavelength λ = 1.550 Å) beam and an incident angle 0.2°, GI XRD was conducted and the pattern was collected with the detector system included a CMOS flat panel X-ray detector C9728DK (52.8 mm square) situated 7.2 cm from the sample position. The scattering wavevector, defined as $q = 4\pi\sin\theta/\lambda$ (with 2θ the scattering angle), was calibrated using silver behenate, sodalite, and silicon powders, respectively.

Computational Details: Quantum−chemical calculations were performed with the Gaussian09 suite employing the WB97XD density functional in combination with the 6−311G(d,p) basis set. Geometry optimizations were performed with tight SCF and convergence criteria and an ultrafine integration grid by applying the GEDIIS optimization algorithm. The minimum nature of each stationary point was confirmed by a frequency analysis.

OFET Device Fabrication and Characterization: An *n*-type heavily doped Si wafer with a SiO_2 layer of 300 nm and a capacitance of 11 nF/cm^2 was used as the gate electrode and dielectric layer. Thin films (40–60 nm in thickness) of polymers were deposited on ODTS treated SiO_2/Si substrates by spin-coating their ODCB solution (5 mg/mL). The thin films were annealed at 200°C for 10 minutes. Gold source and drain contacts (40 nm in thickness) were deposited by vacuum evaporation on the organic layer through a shadow mask, affording a bottom-gate, top-contact OFET device. Electrical measurements of the OFET devices were carried out at room temperature in air using a 4156CSemiconductor Parameter Analyzers, Agilent Technologies. The field-effect mobility was calculated in the saturation regime by using the equation, $I_{ds} = (\mu WC_i/2L)(V_g - V_t)^2$, where I_{ds} is the drain-source current, μ is the field-effect mobility, W is the channel width (1 mm), L is the channel length (0.1 mm), C_i is the capacitance per unit area of the gate dielectric layer, V_g is the gate voltage and V_t is threshold voltage.

BHJ PSC Fabrication and Characterization: The device structures for the conventional PSCs was ITO/PEDOT:PSS/Polymer:$PC_{71}BM$/Ca/Al, and ITO/ZnO/Polymer:$PC_{71}BM$/MoO_3/Ag for the inverted PSCs. The ITO glass substrates were cleaned with detergent, deionized water, acetone, and isopropyl alcohol in an ultrasonic bath and then dried overnight in an oven at >100 °C. In conventional PSCs, substrates were covered by PEDOT:PSS (40 nm; Al 4083 provided by H. C. Stark) using spin-coating, and dried in glove box at 150°C for 30 minutes. Copolymers were dissolved in

ODCB, or ODCB containing 8 v% 1-CN and $PC_{71}BM$ (purchased from Nano-C) was then added into the solution to reach the desired weight ratio. The solution was stirred at 70°C for overnight and filtrated through a 0.45um filter. In a glove box, the solution of polymer:$PC_{71}BM$ was then spin coated to form the active layer. The cathode made of calcium (35 nm) and aluminum (100 nm) was evaporated through a shadow mask under vacuum (<10^{-6} Torr). For the inverted PSCs, zinc acetylacetonate hydrate (purchased from Aldrich) dissolved in methanol (20 mg mL^{-1}) was spin-casted on pre-cleaned ITO substrates and baked at 130 °C for 10 minutes in the air to form the ZnO layer with thickness of 30 nm. The active layer was spin-casted on the ZnO layer using the identical procedure mentioned above. The anode made of MoO_3 (6 nm) and Ag (150 nm) was evaporated through a shadow mask under vacuum (<10^{-6} Torr). Each sample consists of four independent pixels defined by an active area of 0.04 cm^2. The devices were characterized in air under 100 mW/cm^2 AM 1.5 simulated light measurement (Yamashita Denso solar simulator). Current−voltage (*J*−*V*) characteristics of PSC devices were obtained by a Keithley2400 SMU. Solar illumination conforming the JIS Class AAA was provided by a SAN-EI 300W solar simulator equipped with an AM 1.5G filter. The light intensity was calibrated with a Hamamatsu S1336-5BK silicon photodiode.

Transmission Electron Microscopy (TEM) Observation: TEM observations were performed in bright-field, high-resolution mode on a JEOL JEM-2010 transmission electron microscope with an accelerating voltage of 200 kV equipped with a Gatan-831 CCD camera. The thin-film sample was first spun-coated onto a ITO substrate covered with 40 nm of PEDOT:PSS. The sample was then immersed into water to dissolve the PEDOT:PSS layer and separate the thin films from the ITO substrate. Thin films floated on a water surface were picked up by copper grids coated with amorphous carbon layer, dried under vacuum overnight, and used in the TEM observations.

Synthesis of SeFBT: To a round bottom flask was added 5,6-difluoro-4,7-diiodobenzo-2,1,3-thiadiazole1(0.5 g, 1.15 mmol), degassed dry THF (50 mL) and $PdCl_2(PPh_3)_2$ (70 mg, 0.104 mmol). The solution was stirred at 70 °C until all the substance completely dissolved. 2-(tributylstannyl)selenophen(1.33 g, 3.16 mmol) was added dropwise and the mixture was kept at 70 °C for 24 h. After removal of the solvent under reduced pressure, the residue was recrystallized from ethanol to give the product as a red solid. Yield: 450 mg (89%). ^{1}H NMR ($CDCl_3$, 400 MHz): δ (ppm) 8.52 (d, *J* = 3.6 Hz, 2H), 8.36 (d, *J* = 2.4 Hz, 2H), 7.52 (t, *J* = 4.0 Hz, 2H); ^{13}C NMR ($CDCl_3$, 100 MHz): δ (ppm) 110.00, 130.14, 133.00, 133.05, 133.11, 135.37; MS (EI, $C_{14}H_6F_2N_2Se_2S$): Calcd, 430.19; Found, 430.

Synthesis of Sn-SeFBT: To a solution of compound **SeFBT** (300 mg, 0.70 mmol) in dry THF (50 mL) was added a 2 M solution of lithium diisopropylamide in THF (0.87 mL, 1.74 mmol) dropwise at −78 °C. After stirring at −78 °C for 1 h, 1.0 M solution of chlorotrimethylstannane in THF (2.79 mL, 2.79 mmol) was introduced by syringe to the solution. The mixture solution was warmed up to room temperature and stirred for 12 h. After removal of the solvent under reduced pressure,the residue was extracted with diethyl ether (50 mL × 3) and water (50 mL). Solvent was evaporated under reduced pressure and the product as a brown solid was obtained by recrystallization from ethanol. Yield: 300 mg (57%). ^{1}H NMR ($CDCl_3$, 400MHz):□δ (ppm)□8.53 (d, *J* = 4.0 Hz, 2H), 7.68 (d, *J* = 4.0 Hz, 2H), 0.44 (s, 18 H); MS (EI, $C_{20}H_{22}F_2N_2SSe_2Sn_2$): Calcd, 755.80; Found, 755.8.

Synthesis of P(FBT-alt-Se_2Th_2): To a 50 mL round bottom flask was added 5,5'-dibromo-4,4'-bis(2-octyldodecyl)-2,2'-bithiophene (113.3 mg, 0.13 mmol), **Sn-SeFBT** (99.3 mg, 0.13 mmol), tris(dibenzylideneacetone) dipalladium (5.9 mg, 0.0065 mmol), tri(2-methylphenyl)phosphine (15.6 mg, 0.052 mmol) and deoxygenated chlorobenzene (5 mL). The mixture was then degassed by bubbling nitrogen for 10 minutes at room temperature. The round bottom flask was put into the microwave reactor and heated to 180 °C under 270 watt for 50 minutes. Then, tributyl(thiophen-2-yl)stannane (10.5 mg, 0.028 mmol) was added to the mixture solution and reacted for 10 minutes under 270 W. Finally, 2-bromothiophene (20 mg, 0.123 mmol) was added to the mixture solution and reacted for 10 minutes under 270 W. After cooling to room temperature the solution was added dropwise to methanol. The precipitate was collected by filtration and washed by Soxhlet extraction with acetone (24 h), hexane (24 h) and tetrahydrofuran (24 h) sequentially. The residue solid was re-dissolved in hot toluene (150 mL). The Pd-thiol gel (Silicycle Inc. 95.1 mg, 0.11mmol) was added to above toluene solution to remove the residual Pd catalyst at 80 °C for 12 h. After filtration of solution and removal of the solvent under reduced pressure, the polymer solution was added into methanol to re-precipitate. The purified polymer was collected by filtration and dried under vacuum for 1 day to give a black solid. The polymer is soluble in warm chlorinated benzenes, but has poor solubility in tetrahydrofuran and chloroform. Yield: 90 mg (60%).

Results and Discussion

Synthesis of Monomers and Polymers

The synthetic route of **P(FBT-*alt*-Se_2Th_2)** is depicted in the Scheme 1b. Pd-catalyzed Stille-coupling reaction between 5,6-difluoro-4,7-diiodobenzo-2,1,3-thiadiazole (1) and 2-(tributylstannyl)selenophene afforded the formation of 5,6-difluoro-4,7-bis(selenophen-2-yl)benzo-2,1,3-thiadiazole (**SeFBT**) in a 89% yield. Lithiation of the **SeFBT** by lithium diisopropylamide (LDA) followed by reacting with trimethyltin chloride resulted in the formation of 5,6-difluoro-4,7-bis(5-(trimethylstannyl)selenophen-2-yl)benzo-2,1,3-thiadiazole (**Sn-SeFBT**) in 57% yield. **Sn-SeFBT** was then copolymerized with 5,5'-dibromo-4,4'-bis(2-octyldodecyl)-2,2'-bithiophene by Stille-coupling to give the **P(FBT-*alt*-Se_2Th_2)**. The number average molecular weights (M_n) and polydispersity (PDI) are 14.7 kDa and 1.38 for **P(FBT-*alt*-Se_2Th_2)** determined by gel permeation chromatography (GPC) using trichlorobenzene as the eluent at 140 °C.

Optical Absorption, Frontier Orbital Levels and Thermal Behaviors.

The absorption spectra for the **P(FBT-*alt*-Se_2Th_2)** in *o*-dichlorobenzne (ODCB) solution and thin film are shown in Figure 1. In the solution, the absorption bands with λ_{max}s at 430 nm and at 662 nm are attributed to the localized π-π* transition and the photo-induced intramolecular charge transfer (ICT) band of the copolymer. The optical band-gaps (E_g) deduced from the absorption edges of thin film spectrum is 1.56 eV. Compared to **P(FBT-*alt*-Th_4)**[11], **P(FBT-*alt*-Se_2Th_2)** exhibited more bathochromic absorption of the ICT band in solution and solid state due to the selenophenes introducing more quinoidal

character to conjugated polymer backbones.[8d, 9] Deduced from cyclic voltammetry measurement (Figure S1), the E_{HOMO} and E_{LUMO} of **P(FBT-*alt*-Se$_2$Th$_2$)** are − 5.39 eV and − 3.70 eV, respectively. Compared to the E_{HOMO} and E_{LUMO} of **P(FBT-*alt*-Th$_4$)**,[11] the smaller E_g of **P(FBT-*alt*-Se$_2$Th$_2$)** is a result of the elevation of E_{HOMO} as shown in Figure S1b. The result is unexpected, because in the previous cases,[8a, 8d, 8e] the narrower E_g of the -Se- analogues was a result of the deeper-lying E_{LUMO}s instead of the raised E_{HOMO}s. Thus, it is anticipated that the raised E_{HOMO} of **P(FBT-*alt*-Se$_2$Th$_2$)** will decrease the V_{oc} of the **P(FBT-*alt*-Se$_2$Th$_2$)**:$PC_{71}BM$ PSCs.

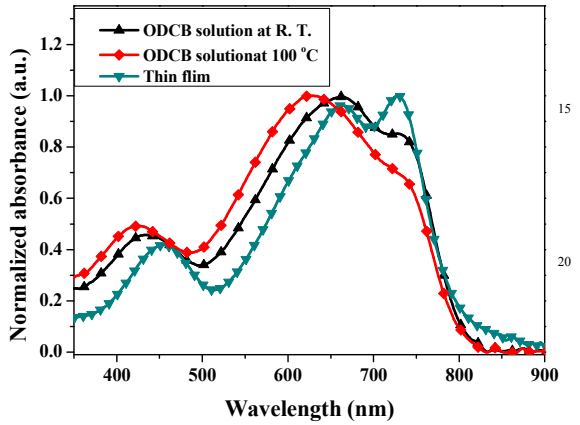

Figure 1. Normalized solution and thin-film UV-vis absorption spectra of the **P(FBT-*alt*-Se$_2$Th$_2$)** copolymers.

As shown in Figure 1, **P(FBT-*alt*-Se$_2$Th$_2$)** thin film exhibited a strong shoulder band with λ_{max} located at 729 nm. The absorption is an indication of better backbone co-planarity and stronger intermolecular interactions of the conjugated chains in the solid-state.[12] Notably, the shoulder band can also be seen in the ODCB solution, which suggests the aggregation of **P(FBT-*alt*-Se$_2$Th$_2$)** chains in the solution. Raise of solution temperature decreases the degree of aggregation and therefore the absorption intensity of the shoulder band.[13] However, **P(FBT-*alt*-Se$_2$Th$_2$)** maintained 81% of the absorption intensity even at a solution temperature of 100 °C. It is much higher than that of **P(FBT-*alt*-Th$_4$)** (43%) in the same condition.[11] **P(FBT-*alt*-Se$_2$Th$_2$)** exhibited good thermal stability with decomposition temperature (T_d) at 435 °C determined from thermogravimetric analysis (Figure S2). The melting temperatures (T_m) of **P(FBT-*alt*-Se$_2$Th$_2$)** was not found below 350 °C in the differential scanning calorimetry measurement. Because wide angle X-ray diffraction (WAXD) study (vide infra) confirms that **P(FBT-*alt*-Se$_2$Th$_2$)** is in its crystalline state at room temperature, the T_m of **P(FBT-*alt*-Se$_2$Th$_2$)** should be above 350 °C, which is higher than the T_m of **P(FBT-*alt*-Th$_4$)** (270 °C). The solution and solid-state behaviors of **P(FBT-*alt*-Se$_2$Th$_2$)** thus suggests that the backbone conformation and the solid-state order of **P(FBT-*alt*-Se$_2$Th$_2$)** are more difficult to be disrupted than its -Th- counterpart.

X-ray Structural Characterization.

Figure 2a shows the powder WAXD patterns of **P(FBT-*alt*-Se$_2$Th$_2$)**. Three diffraction peaks located at 2θ = 2.91°, 5.82° and 8.73° that possess a scattering factor ratio of 1:2:3 were observed. It indicates the presence of a long-range ordered lamellar structure with *d*-spacing of 2.03 nm, and the diffraction peaks can be assigned as the (100), (200) and (300) diffractions for the ordered structure. The diffraction peak located at 2θ = 15.9° (*d*-spacing of 0.37 nm) represents the ordered π − π stacking of **P(FBT-*alt*-Se$_2$Th$_2$)**. Figure 2b show the grazing incidence X-ray diffraction (GI-XRD) pattern of **P(FBT-*alt*-Se$_2$Th$_2$)** thin film. The (100) and (200) diffraction arcs of **P(FBT-*alt*-Se$_2$Th$_2$)** lamellar structure were found along the q_z direction, corresponding to the edge-on lamellar stacking of **P(FBT-*alt*-Se$_2$Th$_2$)** on the substrate surface. The XRD results revealed that the solid-state packing of **P(FBT-*alt*-Se$_2$Th$_2$)** is similar to that of **P(FBT-*alt*-Th$_4$)**, which are both featured with long-range ordered lamellar structure and π − π stacking.[11] It also accounts for the more bathochromic shifts of the ICT bands of both **P(FBT-*alt*-Th$_4$)**[11] and **P(FBT-*alt*-Se$_2$Th$_2$)** in the solid state.

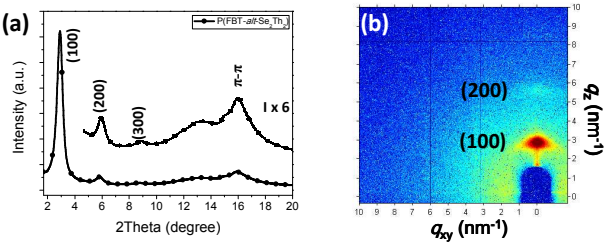

Figure 2. (a) WAXD pattern and (b) GI-XRD pattern of **P(FBT-*alt*-Se$_2$Th$_2$)**.

OFET and BHJ PSC Characteristics.

The μ_h of solution-processed **P(FBT-*alt*-Se$_2$Th$_2$)** thin films were measured using a bottom-gate, top-contact device configuration with evaporated gold source/drain electrodes and octadecyltrichlorosilane (ODTS) modified SiO_2 gate dielectric on n-doped silicon wafer surface. The output and transfer plots (at the same source-drain voltages of − 80 V) of the devices exhibited typical p-channel OFET characteristics (Figure 3). The μ_hs were obtained from the transfer characteristics of the devices in saturation regime. **P(FBT-*alt*-Se$_2$Th$_2$)** exhibited a high μ_h of 0.36 $cm^2V^{-1}s^{-1}$with good on-off ratio of 1.91 × 10^6. Since the solid-state packing of **P(FBT-*alt*-Se$_2$Th$_2$)** and **P(FBT-*alt*-Th$_4$)** are similar, the μ_h of **P(FBT-*alt*-Se$_2$Th$_2$)** is only slightly better than that of **P(FBT-*alt*-Th$_4$)** (μ_h = 0.29 $cm^2V^{-1}s^{-1}$).[11]

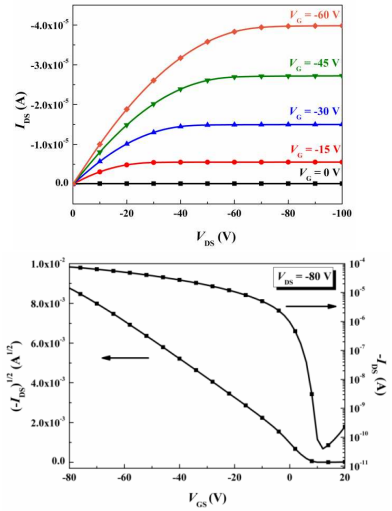

Figure 3.

Typical output curves (up) and transfer plots (down) of the **P(FBT-*alt*-Se$_2$Th$_2$)** OFET devices.

To evaluate the photovoltaic performances of the copolymers, BHJ PSCs with conventional architecture – ITO/PEDOT:PSS/**P(FBT-*alt*-Se$_2$Th$_2$)**:PC$_{71}$BM (1:1 in wt %)/Ca/Al and inverted architecture – ITO/ZnO/**P(FBT-*alt*-Se$_2$Th$_2$)**:PC$_{71}$BM (1:1 in wt %)/MoO_3/Ag were fabricated. Their performances were measured under a simulated AM 1.5 G illumination of 100 mW/cm^2. The current density-voltage characteristics of the devices are shown in Figure 4 and summarized in Table 1. In the conventional architecture, **P(FBT-*alt*-Se$_2$Th$_2$)**:PC$_{71}$BM PSCs delivered a moderate PCE of 5.47% with a V_{oc} of 0.68 V, a J_{sc} of 12.5 mA/cm^2, and a FF of 64.3%. Unexpectedly, the narrower E_g of **P(FBT-*alt*-Se$_2$Th$_2$)** did not promote a higher J_{sc} than those given by the **P(FBT-*alt*-Th$_4$)**:PC$_{71}$BM PSCs.[11]

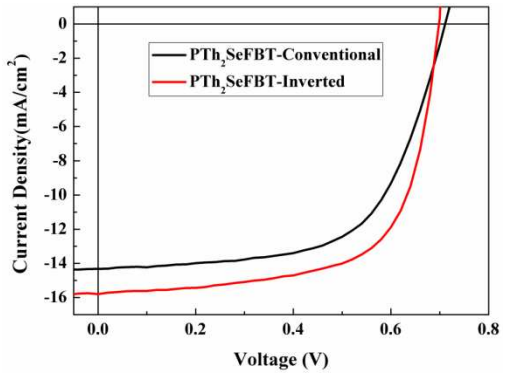

Figure 4. Current density-voltage characteristics of the **P(FBT-*alt*-Se$_2$Th$_2$)**:PC$_{71}$BM based BHJ PSCs in the conventional and inverted device architectures under illumination of AM 1.5 G at 100 mW/cm^2.

Table 1. PSCs Characteristics of the **P(FBT-*alt*-Se$_2$Th$_2$)**:PC$_{71}$BM BHJ PSCs

Architecture	V_{oc} (V)	J_{sc} (mA/cm^2)	*FF* (%)	PCE (%)
Conventional	0.68	12.5	64.3	5.47
Conventional[a]	0.72	14.3	61.2	6.31
Inverted[a]	0.70	15.8	66.4	7.34

[a]With 8 v% of 1-CN as additive.

To identify the origins of the low J_{sc}, morphological analysis of the **P(FBT-*alt*-Se$_2$Th$_2$)**:PC$_{71}$BM thin-film was carried out in HR-TEM. As shown in Figure 5a, deep dark spots were observed in the **P(FBT-*alt*-Se$_2$Th$_2$)**:PC$_{71}$BM thin film prepared from the ODCB solution. The deep dark spots were assigned as the polymer-rich domains, because of the higher atomic scattering factor of the selenium atoms of **P(FBT-*alt*-Se$_2$Th$_2$)**. Figure 5b shows the image of the dark spot at a higher magnification. Stacks of dark lines, which are separated uniformly with a distance of ~0.37 nm, were observed inside the dark spot. The distance matches the *d*-spacing of the π-π stacking, and further confirmed the dark regions as the polymer-rich domains. The results indicated that **P(FBT-*alt*-Se$_2$Th$_2$)** tends to segregate into large domains in the active layer. To decrease the degree of segregation, 1-CN was used as additive. With 8 v% of 1-CN, the population of large dark spots decreased as shown in Figure 5c. A more homogenous morphology, which contains interpenetrating polymer-rich (darker regions), and polymer-deficient (brighter regions) was obtained. Although deep dark spots can still be observed in the thin-film (Figure 5d), their sizes are significantly decreased. Therefore, 1-CN effectively suppressed the segregation of **P(FBT-*alt*-Se$_2$Th$_2$)**, and facilitates the formation of a more homogenous active morphology.

The morphological changes increased the J_{sc} of the **P(FBT-*alt*-Se$_2$Th$_2$)**:PC$_{71}$BM PSCs. The PSCs prepared with 8 v% of 1-CN gave a J_{sc} of 14.3 mA/cm^2 and a PCE of 6.31%. In inverted PSCs, an even higher PCE of 7.34% with a V_{oc} of 0.70 V, a J_{sc} of 15.8 mA/cm^2, and a FF of 66.4% was delivered. Compared to **P(FBT-*alt*-Th$_4$)**:PC$_{71}$BM PSCs, which delivered a PCE of 6.82% with a V_{oc} of 0.77 V, a J_{sc} of 13.5 mA/cm^2, and a FF of 65.6%,[11] the higher-lying E_{HOMO} of **P(FBT-*alt*-Se$_2$Th$_2$)** caused negative impact to the V_{oc}. However, when the morphology of the **P(FBT-*alt*-Se$_2$Th$_2$)**:PC$_{71}$BM active thin film is optimized, the narrower E_g of **P(FBT-*alt*-Se$_2$Th$_2$)** promoted the J_{sc} and resulted in an overall higher PCE of over 7%.

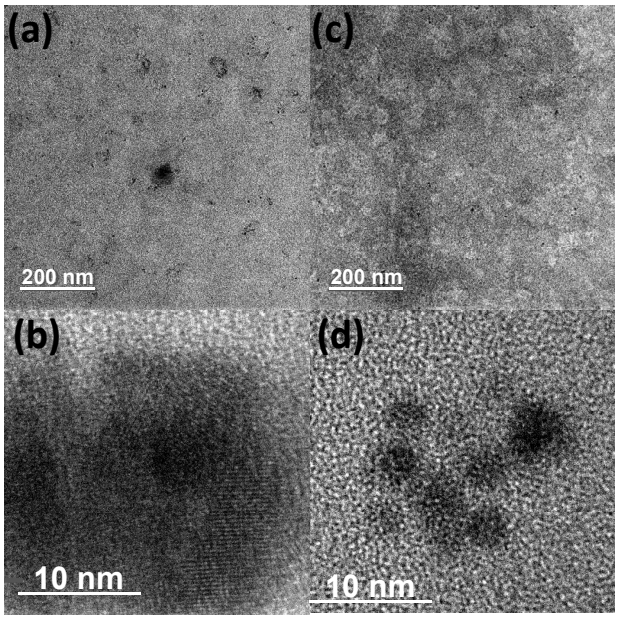

Figure 5. HR-TEM images of the **P(FBT-*alt*-Se$_2$Th$_2$)**:PC$_{71}$BM(1:1 in wt %) thin films prepared from a ODCB solution at (a) 50k× and (b) 400k× magnifications; **P(FBT-*alt*-Se$_2$Th$_2$)**:PC$_{71}$BM (1:1 in wt %) thin films prepared from a ODCB solution with 8 v% 1-CN at (c) 50k× and (d) 400k× magnifications.

Theoretical Calculations of the P(FBT-*alt*-CP$_4$) Copolymers.

The molecular properties, solution and solid-state behaviors of **P(FBT-*alt*-Se$_2$Th$_2$)** and **P(FBT-*alt*-Th$_4$)** revealed the remarkable influences of the -CP- π-bridges to the properties of the **P(FBT-*alt*-CP$_4$)** copolymers. The much stronger aggregation tendency of **P(FBT-*alt*-Se$_2$Th$_2$)** significantly affected the solid-state morphology and consequently the performances of the copolymers. Intermolecular non-covalent interactions and

molecular geometries are both essential in the aggregation and self-assembly processes.[14] To understand the possible causes of the different aggregation strengths, the dipole moments of the **SeFBT** structural units, and the optimized conformations of the repeat units of **P(FBT-*alt*-Se$_2$Th$_2$)** and **P(FBT-*alt*-Th$_4$)** were further investigated through theoretical calculations.

Figure S3 shows the optimized structures and the calculated dipole moments of **SeFBT**. The result was obtained via theoretical calculations performed with the Gaussian09 suite employing the WB97XD density functional in combination with the 6-311G(d,p) basis set. It was found that the dipole moments of **SeFBT** are comparable to that of 5,6-difluoro-4,7-di(thiophen-2-yl)benzo-2,1,3-thiadiazole (**ThFBT**).[11] Thus, the variation in the π-bridges does not significantly change the dipole moments of the acceptor structural units. In this case, the stronger aggregation tendency of **P(FBT-*alt*-Se$_2$Th$_2$)** cannot be simply attributed to difference in the molecular dipole moment. Figure 6 shows the optimized conformations of the repeat units of the two **P(FBT-*alt*-CP$_4$)** copolymers. The conformations were obtained through theoretical calculation at the WB97XD/6-311G(d,p) level of density functional theory. The 2-octyldodecyl side chains were replaced by isobutyl groups to keep the branched geometry of the alkyl groups, but avoid excessive computation demand. The calculated bond angles (θ) and bond lengths (L) were summarized in Table 2. θ_1 and θ_2 are the interannual dihedral angles between the CP unit and its neighboring aromatic units. These angles are nearly identical in both repeat units. Therefore, as can be seen from the side view in Figure 6, the coplanarity of both repeat units in their optimized geometries is similar. The main geometrical difference in the repeat units can be found within the -Th- and the -Se- units. Because the van der Waals radius of selenium (1.90 Å) is larger than that of sulfur (1.80 Å),[15] the -Se- unit has longer carbon-heteroatom bonds (L_1 and L_2), and a wider included angle θ_3. Along the chain axis, the wider θ_3 makes the repeat unit of **P(FBT-*alt*-Se$_2$Th$_2$)** less curved than that of **P(FBT-*alt*-Th$_4$)**, as can be seen from the top view of the repeat units in Figure 6. In summary, the theoretical calculations indicates that the variation in the -CP- π-bridges affects more on the linearity of the repeat units than on the molecular dipole moment and the coplanarity of the repeat units. Thus, it is likely that **P(FBT-*alt*-Se$_2$Th$_2$)** possess stronger aggregation strength because of its more linear backbone geometry. The interannular bond lengths of the repeat units were also and summarized in Table S1. These lengths are essentially identical in both repeat units.

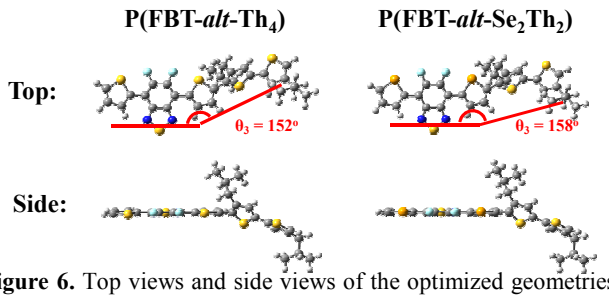

Figure 6. Top views and side views of the optimized geometries of the repeat units of **P(FBT-*alt*-Th$_4$)** and **P(FBT-*alt*-Se$_2$Th$_2$)** at the WB97XD/6-311G(d,p) level of theory. The atoms are shown in the following colors: sulfur (yellow), selenium (orange), fluorine (light blue), carbon (gray), nitrogen (blue), and hydrogen (light gray).

Table 2. Calculated bond lengths, bond angles, and dihedral angles of the repeat units of the **P(FBT-*alt*-CP$_4$)** copolymers.[a]
[a] Illustration and definition of θ_1, θ_2, θ_3, L_1, and L_2.

	X	θ_1 (deg)	θ_2 (deg)	θ_3 (deg)	L_1 (Å)	L_2 (Å)
P(FBT-*alt*-Th$_4$)	S	2.6	–50.2	152	1.75	1.73
P(FBT-*alt*-Se$_2$Th$_2$)	Se	–0.7	–50.7	158	1.89	1.87

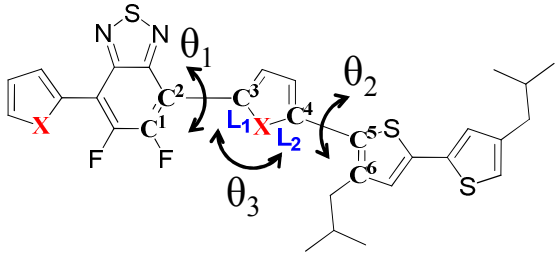

θ_1: dihedral angle of C_1–C_2–C_3–X, θ_2: dihedral angle of X–C_4–C_5–C_6, θ_3: included angle between C_2–C_3 and C_4–C_5 bonds, L_1: bond length of C_3-X bond, L_2: bond length of X-C_4 bond.

Conclusions

An novel **P(FBT-*alt*-CP$_4$)** copolymer, **P(FBT-*alt*-Se$_2$Th$_2$)**, was designed and synthesized. Compared to its -Th- analogue, **P(FBT-*alt*-Se$_2$Th$_2$)**, possesses a smaller E_g, and an elevated E_{HOMO}. **P(FBT-*alt*-Se$_2$Th$_2$)** strongly aggregates in solution and packed into long-range ordered lamellar structure and π-π stacking in the solid-state. The T_m of ordered phase is above 350 °C. Because of its high solid-state order, **P(FBT-*alt*-Se$_2$Th$_2$)** delivered high OFET μ_h of 0.36 $cm^2V^{-1}s^{-1}$. When applied to BHJ PSCs, **P(FBT-*alt*-Se$_2$Th$_2$)** segregates into large domains in the **P(FBT-*alt*-Se$_2$Th$_2$)**:$PC_{71}BM$ thin film. Addition of 8 v% of 1-CN additive prevented strong aggregation of **P(FBT-*alt*-Se$_2$Th$_2$)** and drove the active layer morphology toward ideal bi-continuous interpenetrating network, which consequently promoted the PCE. A superior PCE of 7.34% with a V_{oc} of 0.70 V, a J_{sc} of 15.8 mA/cm^2, and a FF of 66.4% was delivered in the inverted **P(FBT-*alt*-Se$_2$Th$_2$)**:$PC_{71}BM$ PSC. Theoretical calculations showed that the repeat unit containing the -Se- π-bridges is more linear than the one with the -Th- π-bridges. The strong aggregation strength of **P(FBT-*alt*-Se$_2$Th$_2$)** is thus likely related to its more straight conjugated backbone.

Notes and references

Department of Applied Chemistry, National Chiao Tung University, 1001Ta Hsueh Rd., Hsinchu, Taiwan 30010

**Corresponding author: cshsu@mail.nctu.edu.tw; kclwang@nctu.edu.tw*

† Electronic Supplementary Information (ESI) available: [details of any supplementary information available should be included here]. See DOI: 10.1039/b000000x/

Acknowledgement

This work is supported by the National Science Council and "ATP" of the National Chiao Tung University and Ministry of

Education, Taiwan. The authors thank Prof. Keng S. Liang at Institute of Physics, Academia Sinica, Taiwan; Mr. Chi-Feng Huang at the Department of Applied Chemistry, National Chiao Tung Univerisity; Dr. Hwo-Shuenn Sheu at beamline BL01C; Dr. U-Ser Jeng and Dr. Chun-Jen Su at beamline BL23A of the National Synchrotron Radiation Research Center (NSRRC) in Taiwan for assistance with the XRD measurements.

References

1 M. C. Scharber, D. Wuhlbacher, M. Koppe, P. Denk, C. Waldauf, A. J. Heeger and C. L. Brabec, *Adv. Mater*., 2006, **18**, 789.

2 (*a*) H. Zhou, L. Yang, A. C. Stuart, S. C. Price, S. Liu and W. You, *Angew. Chem. Int. Ed.,* 2011, **50**, 2995; (*b*) C. M. Amb, S. Chen, K. R. Graham, J. Subbiah, C. E. Small, F. So and J. R. Reynolds, *J. Am. Chem. Soc*., 2011, **133**, 10062; (*c*) C.-Y. Chang, Y.-J. Cheng, S.-H. Hung, J.-S. Wu, W.-S. Kao, C.-H. Lee and C.-S. Hsu, *Adv. Mater.*, 2012, **2**, 549; (*d*) S. C. Price, A. C. Stuart, L. Yang, H. Zhou and W. You, *J. Am. Chem. Soc.*, 2011, **133**, 4625; (*e*) H. Y. Chen, J. H. Hou, S. Q. Zhang, Y. Y. Liang, G. W. Yang, Y. Yang, L. P. Yu, Y. Wu and G. Li, *Nat. Photonics,* 2009, **3**, 649; (*f*) I. Osaka, T. Kakara, N. Takemura, T. Koganezawa and K. Takimiya, *J. Am. Chem. Soc*., 2013, **135**, 8834; (*g*) H. Zhong, Z. Li, F. Deledalle, E. C. Fregoso, M. Shahid, Z. Fei, C. B. Nielsen, N. Yaacobi-Gross, S. Rossbauer, T. D. Anthopoulos, J. R. Durrant and M. Heeney, *J. Am. Chem. Soc.*, 2013, **135**, 2040; (*h*) H. J. Son, L. Lu, W. Chen, T. Xu, T. Zheng, B. Carsten, J. Strzalka, S. B. Darling, L. X. Chen and L. Yu, *Adv. Mater.*, 2013, **25**, 838; (*i*) Y.-X. Xu, C. C. Chueh, H.-L. Yip, F.-Z. Ding, Y.-X. Li, C.-Z. Li, X. Li, W.-C. Chen and A. K.-Y. Jen, *Adv. Mater.*, 2012, **24**, 6356; (*j*) J. Cao, Q. Liao, X. Du, J. Chen, Z. Xiao, Q. Zuo and L. Ding, *Energy Environ. Sci*., 2013, **6**, 3224; (*k*) Y. Li, P. Sonar, L. Murphy and W. Hong, *Energy Environ. Sci.*, 2013, **6**, 1684; (*l*) J. W. Jung, F. Liu, T. P. Russell and W. H. Jo, *Energy Environ. Sci.*, 2013, **6**, 3301; (*m*) Y. Li, *Acc. Chem. Res*., 2012, **45**, 723; (*n*) L. Huo, S. Zhang, X. Guo, F. Xu, Y. Li and J. Hou, *Angew. Chem. Int. Ed.,* 2011, **50**, 9697.

3 (*a*) H. Xin, X. Guo, G. Ren, M. D. Watson and S. A. Jenekhe, *Adv. Energy Mater*., 2012, **2**, 575; (*b*) S. Kwon, J. K. Park, G. Kim, J. Kong, G. C. Bazan and K. Lee, *Adv. Energy Mater.*, 2012, **2**, 1420; (*c*) Y. Liang, Z. Xu, J. Xia, S.-T. Tsai, Y. Wu, G. Li, C. Ray and L. Yu, *Adv. Mater.*, 2010, **22**, E135; (*d*) J. T. Rogers, K. Schmidt, M. F. Toney, E. J. Kramer and G. C. Bazan, *Adv. Mater.*, 2011, **23**, 2284; (*e*) J. K. Lee, W. L. Ma, C. J. Brabec, J. Yuen, J. S. Moon, J. Y. Kim, K. Lee, G. C. Bazan and A. J. Heeger, *J. Am. Chem. Soc.*, 2008, **130**, 3619; (*f*) S. J. Lou, J. M. Szarko, T. Xu, L. Yu, T. J. Marks and L. X. Chen, *J. Am. Chem. Soc.*, 2011, **133**, 20661; (*g*) J. S. Moon, C. J. Takacs, S. Cho, R. C. Coffin, H. Kim, G. C. Bazan and A. J. Heeger, *Nano Lett.*, 2010, **10**, 4005; (*h*) J. Peet, J. Y. Kim, N. E. Coates, W. L. Ma, D. Moses, A. J. Heeger and G. C. Bazan, *Nat. Mater*., 2007, **6**, 497; (*i*) H.-C. Liao, C.-S. Tsao, Y.-T. Shao, S.-Y. Chang, Y.-C. Huang, C.-M. Chuang, T.-H. Lin, C.-Y. Chen, C.-J. Su, U. S. Jeng, Y.-F. Chen and W.-F. Su, *Energy Environ. Sci.*, 2013, **6**, 1938; (*j*) M. Pfannmoller, W. Kowalsky and R. R. Schroder, *Energy Environ. Sci.*, 2013, **6**, 2871.

4 (*a*) Z. He, C. Zhong, X. Huang, W.-Y. Wong, H. Wu, L. Chen, S. Su and Y. Cao, *Adv. Mater.*, 2011, **23**, 4636; (*b*) S.-H. Liao, H.-J. Jhuo, Y.-S. Cheng and S.-A. Chen, *Adv. Mater.*, 2013, **25**, 4766; (*c*) Y.-J. Cheng, C.-H. Hsieh, T. He, C.-S. Hsu and Y. Li, *J. Am. Chem. Soc.*, 2010, **132**, 17381; (*d*) C.-H. Hsieh, Y.-J. Cheng, P.-J. Li, C.-H. Chen, M. Dubosc, R.-M. Liang, C.-S. Hsu, *J. Am. Chem. Soc.*, 2010, **132**, 4887; (*e*) K. M. O'Malley, C.-Z. Li, H.-L. Yip, A. K.-Y. Jen, *Adv. Energy Mater*., 2012, **2**, 82; (*f*) C.-Y. Chang, L. Zuo, H.-L. Yip, Y. Li, C.-Z. Li, C.-S. Hsu, Y.-J. Cheng, H. Chen and A. K.-Y. Jen, *Adv. Funct. Mater.*, 2013, **23**, 5084.

5 (*a*) J. You, C.-C. Chen, Z. Hong, K. Yoshimura, K. Ohya, R. Xu, S. Ye, J. Gao, G. Li and Y. Yang, *Adv. Mater.*, 2013, **25**, 3973; (*b*) J. You, L. Dou, K. Yoshimura, T. Kato, K. Ohya, T. Moriarty, K. Emery, C.-C. Chen and J. Gao, *Nat. Commun*., 2013, **4**, 1446; (*c*) O. Adebanjo, P. Maharjan, P. Adhikary, M. Wang, S. Yang and Q. Qiao, *Energy Environ. Sci.*, 2013, **6**, 3150; (*d*) T. Ameri, N. Li and C. J. Brabec, *Energy Environ. Sci.*, 2013, **6**, 2390; (*e*) C.-C. Chen, L. Dou, J. Gao, W.-H. Chang, G. Li and Y. Yang, *Energy Environ. Sci.*, 2013, **6**, 2714.

6 (*a*) C. H. Woo, P. M. Beaujuge, T. W. Holcombe, O. P. Lee and J. M. J. Fréchet, *J. Am. Chem. Soc.,* 2010, **132**, 15547; (*b*) A. T. Yiu, P. M. Beaujuge, O. P. Lee, C. H. Woo, M. F. Toney and J. M. J. Fréchet, *J. Am. Chem. Soc.,* 2012, **134**, 2180; (*c*) B. M. Kobilka, B. J. Hale, M. D. Ewan, A. V. Dubrovskiy, T. L. Nelson, V. Duzhko and M. Jeffries-EL, *Polym. Chem.,* 2013, **4**, 5329.

7 X. Wang, S. Chen, Y. Sun, M. Zhang, Y. Li, X. Li and H. Wang, *Polym. Chem*., 2011, **2**, 2872.

8 (*a*) M. Heeney, W. Zhang, D. J. Crouch, M. L. Chabinyc, S. Gordeyev, R. Hamilton, S. J. Higgins, I. McCulloch, P. J. Skabara, D. Sparrowe and S. Tierney, *Chem. Commun.*, 2007, 5061; (*b*) S. S. Zade, N. Zamoshchik and M. Bendikov, *Chem. Eur. J*., 2009, **15**, 8613; (*c*) Z. Chen, H. Lemke, S. Albert-Seifried, M. Caironi, M. M. Nielsen, M. Heeney, W. Zhang, I. McCulloch and H. Sirringhaus, *Adv. Mater.*, 2010, **22**, 2371; (*d*) B. Kim, H. R. Yeom, M. H. Yun, J. Y. Kim and C. Yang, *Macromolecules*, 2012, **45**, 8658; (*e*) A. A. B. Alghamdi, D. C. Watters, H. Yi, S. Al-Faifi, M. S. Almeataq, D. Coles, J. Kingsley, D. G. Lidzey and A. Iraqi, *J. Mater. Chem. A*, 2013, **1**, 5165.

9 (*a*) H.-Y. Chen, S.-C. Yeh, C.-T. Chen and C.-T. Chen, *J. Mater. Chem.,* 2012, **22**, 21549; (*b*) S. S. Zade, N. Zamoshchik and M. Bendikov, *Chem. Eur. J.*, 2009, **15**, 8613.

10 (*a*) J. S. Ha, K. H. Kim and D. H. Choi, *J. Am. Chem. Soc*., 2011, **133**, 10364; (*b*) M. Shahid, T. McCarthy-Ward, J. Labram, S. Rossbauer, E. B. Domingo, S. E. Watkins, N. Stingelin, T. D. Anthopoulos and M. Heeney, *Chem. Sci*., 2012, **3**, 181; (*c*) J. D. Yuen and F. Wudl, *Energy Environ. Sci*., 2013, **6**, 392; (*d*) D. H. Wang, A. Pron, M. Leclerc and A. J. Heeger, *Adv. Funct. Mater.*, 2013, **23**, 1297; (*e*) L. Dou, W.-H. Chang, J. Gao, C.-C. Chen, J. You and Y. Yang, *Adv. Mater.*, 2013, **25**, 825; (*f*) M. Shahid, R. S. Ashraf, Z. Huang, A. J. Kronemeijer, T. McCarthy-Ward, I. McCulloch, J. R. Durrant, H. Sirringhaus and M. Heeney, *J. Mater. Chem.*, 2012, **22**, 1281; (*g*) A. J. Kronemeijer, E. Gili, M. Shahid, J. Rivnay, A. Salleo, M. Heeney and H. Sirringhaus, *Adv. Mater.*, 2012, **24**, 1558.

11 J.-F. Jheng, Y.-Y. Lai, J.-S. Wu, Y.-H. Chao, C.-L. Wang and C.-S. Hsu, *Adv. Mater.*, 2013, **25**, 2445.

12 C. Yang, F. P. Orfino and S. Holdcroft, *Macromolecules*, 1996, **29**, 6510.

13 (*a*) B. P. Karsten, L. Viani, J. Gierschner, J. r. m. Cornil and R. A. J. Janssen, *J. Phys. Chem. A*, 2008, **112**, 10764; (*b*) R. Traiphol, N. Charoenthai, T. Srikhirin, T. Kerdcharoen, T. Osotchan and T. Maturos, *Polymer*, 2007, **48**, 813; (*c*) A. P. Zoombelt, M. Fonrodona, M. G. R. Turbiez, M. M. Wienk and R. A. J. Janssen, *J. Mater. Chem.*, 2009, **19**, 5336. (*d*) R. C. Coffin, J. Peet, J. Rogers and G. C. Bazan, *Nature Chem.*, 2009, **1**, 657; (*e*) R. Steyrleuthner, M. Schubert, I. Howard, B. Klaumünzer, K. Schilling, Z. Chen, P. Saalfrank, F. Laquai, A. Facchetti and D. Neher, *J. Am. Chem. Soc.*, 2012, **134**, 18303.

14 (*a*) S. E. Wheeler, *Acc. Chem. Res.*, 2013, **46**, 1029; (*b*) C. D. Sherrill, *Acc. Chem. Res.*, 2013, **46**, 1020.

15 A. Bondi, *J. Phys. Chem.*, 1964, **68**, 441.

Table of Contents

A superior PCE of 7.34% was delivered in the inverted **P(FBT-*alt*-Se_2Th_2)**:$PC_{71}BM$ polymer solar cells. The strong aggregation of **P(FBT-*alt*-Se_2Th_2)** is likely related to its more straight conjugated backbone according to the theoretical calculation results of the **FBT-*alt*-Se_2Th_2** repeat unit.

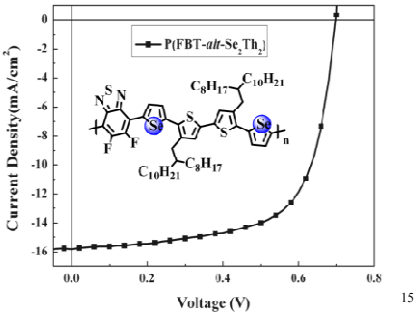

V_{oc} = 0.70 V

J_{sc} = 15.80 mA/cm^2

FF = 66.4 %

PCE = 7.34 %

Mobility = 0.36 cm^2 V^{-1}s^{-1}